Material Properties' Influence in Fuel-Coolant Interaction Codes

Mitja Uršič

Matjaž Leskovar

Borut Mavko

Jožef Stefan Institute,
Jamova cesta 39,
1001 Ljubljana, Slovenia

The melt droplets' crust formation modeling, which is used in current fuel coolant interaction (FCI) codes, is rather basic. In the paper the development of the melt droplet heat transfer model, which enables the treatment of the material properties' influence on the steam explosion, is presented. The model is complex enough to adequately predict the crust development during the melt droplets' cooling in the premixing phase. At the same time the model is simple enough that it can be practically implemented into FCI codes and is thus being an optimal model for FCI applications. Fragmentation criteria are derived in order to take into account the influence of the formed crust on the steam explosion process. The derived criteria are based on experimental results and the thin plate approximation. To enable the use of the model and the fragmentation criteria in FCI codes with Eulerian formulation, adequate transport equations for model parameters are given. [DOI: 10.1115/1.4000339]

1 Introduction

A steam explosion may occur during a hypothetical severe reactor accident in a nuclear power plant, when the molten core (corium) interacts with the water [1]. In this energetic FCI process part of the corium energy is intensively transferred to the water in a very short time scale. The water vaporizes at high pressure and expands, inducing potentially severe dynamic loadings on surrounding systems, structures, and components. Although safety analyses of nuclear power plants revealed a low probability of steam explosion occurrence as a severe reactor accident consequence, steam explosions are an important nuclear safety issue since they can potentially jeopardize the primary system and the containment integrity of the nuclear power plant [2,3]. Direct or by-passed loss of the containment integrity can lead to radioactive material release into the environment, threatening the safety of the general public.

Steam explosion experiments have revealed important differences in behavior between simulant (e.g., Al_2O_3) and prototypical melts (e.g., corium-mixture of UO_2 and ZrO_2) [4,5]. The steam explosion energy efficiency for prototypic melts ($\sim$0.1%) is significantly lower than for simulant melts ($\sim$1%). Additionally, the experimental results have shown that the energy efficiency of prototypic melts strongly depends on the composition of the corium. In the case of the eutectic corium composition the steam explosion can trigger spontaneously with efficiency up to 0.4%, whereas for noneutectic compositions the steam explosion never triggered spontaneously and the energetics of triggered explosions was much lower (efficiency $\sim$0.02%). Differences in the material properties shown in Table 1 are one of the probable reasons for the observed differences in the steam explosion efficiency of prototypic melts in comparison to simulant melts [5].

The influence of the material properties on the premixing, triggering, escalation, and propagation of the steam explosion is very complex (Fig. 1) [5,7]. Namely, several FCI processes depend on the material properties. The influence of material properties may be either positive or negative, leading finely to an increase or a decrease in the ability to trigger an explosion (triggerability), the ability of the explosion to escalate and propagate through the premixture (explosivity), and the efficiency of the conversion of the melt thermal energy to mechanical work (energetics). With a higher density the melt penetrates faster through water and the melt jet breaks up into smaller droplets. Since smaller droplets have a larger surface and consequently a larger area for fine fragmentation, this results in an increase in the explosivity and the energetics. On the other hand, a larger melt droplets' surface means also a larger heat transfer area resulting in a high void buildup, which reduces the triggerability, the explosivity, and the energetics due to the water's depletion and compressibility effects. A small droplet size means also faster crust formation and solidification, which inhibits the fine fragmentation and consequently reduces the triggerability, the explosivity, and the energetics. The crust formation is promoted also by low thermal conductivity and a low specific and latent heat. With a high melt temperature the radiative heat flux is high, which results in a high local void fraction. In addition with a high melt temperature also the vapor film around the melt drops is stabilized, which reduces the probability of the melt-water contact and consequently the triggerability. But with a high melt temperature also the energy of the melt is high, which can result in a more energetic explosion. The melt energy is higher also with higher specific and latent heat and with higher density. For some materials additional energy is released to the melt by the melt's oxidation in the water's vapor. During the oxidation hydrogen is produced, which has a promoting and an inhibiting influence on the steam explosion at the same time. Since hydrogen is a noncondensable gas it cannot condense and therefore the expansion process is more complete, which increases the energetics. But on the other hand hydrogen increases the stability of the vapor film and increases the void fraction, which reduces the triggerability, the explosivity, and the energetics. If the melt composition is noneutectic a mush region may form. A stiff, highly viscous mushy layer suppresses the fine fragmentation and so decreases the triggerability, the explosivity, and the energetics of the steam explosion.

The experimentally observed differences in behavior between melt materials are mainly attributed to differences in crust formation during the premixing phase. The crust formation is believed to be one of the most decisive consequences of the material properties, which limit the strength of the steam explosion [5]. Namely, the crust inhibits the fine fragmentation process during the explosion phase and if the crust is thick enough it completely prevents it. Therefore, the crust formation during the premixing phase could explain the observed differences in the steam explosion efficiency between simulant alumina and prototypic corium melts [8].

In FCI codes the crust formation is simulated with melt droplet heat transfer models. The melt droplet heat transfer models used

Contributed by the Nuclear Division of ASME for publication in the JOURNAL OF ENGINEERING FOR GAS TURBINES AND POWER. Manuscript received July 20, 2009; final manuscript received September 3, 2009; published online April 26, 2010. Editor: Dilip R. Ballal.

Table 1 Selected typical physical parameters of alumina and corium (Refs. [5,6])

Material property	Alumina	Corium
Melting temperature, T_m (K)	2334	2800
Density, ρ (kg/m^3)	2600	8000
Liquid specific heat, c_l (J/kg/K)	1420	520
Solid specific heat, c_s (J/kg/K)	1370	380
Thermal conductivity, λ (W/m/K)	8	2.88
Latent heat, L (kJ/kg)	1198	361
Emissivity in water, ε	0.76	0.76

in complex FCI codes are currently rather basic [9]. Namely, a high complexity of the model would improve the accuracy of the FCI codes, but would be on the other hand generally unpractical due to a significant increase in the computational requirements. It is believed that an improvement in the accuracy of the melt droplet heat transfer model would give a noticeable improvement in the prediction of the steam explosion energetics and also in the prediction of the differences in the energetics between simulant and prototypic melts. Therefore the model for melt droplet heat transfer should be simple enough to be practical for the implementation into FCI codes and complex enough to adequately implement material properties, and finally it should enable the simulation of the limitations to fine fragmentation as a result of the crust formation during premixing. It is believed that an improvement in the accuracy of the melt droplet solidification modeling would enable to reduce the discovered safety significant uncertainties in the prediction of pressure loads during a steam explosion in reactor conditions.

In the paper the development of a reasonable complex melt droplets' heat transfer model, which is able to predict the solid crust growth on the melt droplets' surface and the droplets' surface temperature during the premixing phase, considering the melt material properties, is presented. Additionally, to consider the influence of the formed solid crust on the fragmentation process, an appropriate fragmentation criterion is proposed, to enable to determine whether melt droplets' coarse breaks up and fine fragmentation may occur during the premixing and explosion phases, respectively. To enable the use of the developed melt droplet heat transfer model and the fragmentation criteria in FCI computer codes with an Eulerian description, adequate conservative transport equations for the most important model parameters are also presented.

2 Melt Droplets' Heat Transfer Model

2.1 Mathematical-Physical Background. Thermal radiation is an important mode of heat transfer from the melt droplets to the ambient water during the cooling and solidification of the melt droplets. When the droplets are transparent for thermal radiation, the thermal radiation comes from the whole droplet volume. On the other hand if the droplet is opaque for thermal radiation, the particle is cooled by radiation only from the surface of the droplet. If the absorption coefficient and the typical radius of the melt droplets are taken into consideration, then typical droplets from simulant alumina and prototypic corium melts may be considered as opaque, since for both materials the typical melt droplets' radius (around 1 mm for corium and around 10 mm for alumina) is much larger in comparison with the absorption length (around 0.2 mm for corium and around 1 mm for alumina) [4,8]. Due to that, the modeling must be based on a mathematical-physical model for opaque droplets [10].

In the mathematical-physical modeling of opaque droplets a model problem for a single melt droplet is considered, since the heat transfer between melt droplets' particles is assumed to be insignificant compared with the local heat transfer to the surrounding water. The transient heat conduction equation for an opaque spherical droplet together with the boundary and initial conditions is

$$\rho(c[T] + L\delta[T - T_m])\frac{\partial T[r,t]}{\partial t} = \lambda \nabla^2 T[r,t]$$

$$T[r,0] = T_{\text{cen}}[t=0], \qquad \left.\frac{\partial T}{\partial r}\right|_{r=0} = 0, \qquad -\lambda \left.\frac{\partial T}{\partial r}\right|_{r=R} = q[t] \quad (1)$$

where $T[r,t]$ is the temperature profile inside the particle with radius R, and c is the specific heat capacity. The other variables are described in Table 1 and are assumed to be constant. Since the eutectic melt composition is considered, the liquidus (completely liquid) and solidus (completely solid) temperatures are identical and equal to the melting temperature (i.e., δ is the delta function). $T_{\text{cen}}[t=0]$ is a homogenous temperature profile defining the initial droplets' temperature at the beginning of the droplets' cooling. The first boundary condition assumes that there are no heat sources in the center of the droplet. The second boundary condition equals the heat flux due to the temperature profile gradient at the melt droplet surface to the heat flux q from the surface of the melt droplet to the surrounding water.

2.2 Model Description. Equation (1) has analytical solutions only for specific initial and boundary conditions, which in general do not represent situations in steam explosion processes. Since a numerical solution (NS) of Eq. (1) would increase the computational requirements of the FCI codes too much and is therefore unacceptable, the concept of the reasonable complex melt droplets' heat transfer model for opaque droplets (HTMOD), as illustrated in Fig. 2, was introduced in Ref. [10]. With HTMOD we would like to reach a reasonable compromise between the accuracy and the computational efficiency of melt droplets' heat transfer calculations. As shown in Fig. 2 the melt droplet with radius R

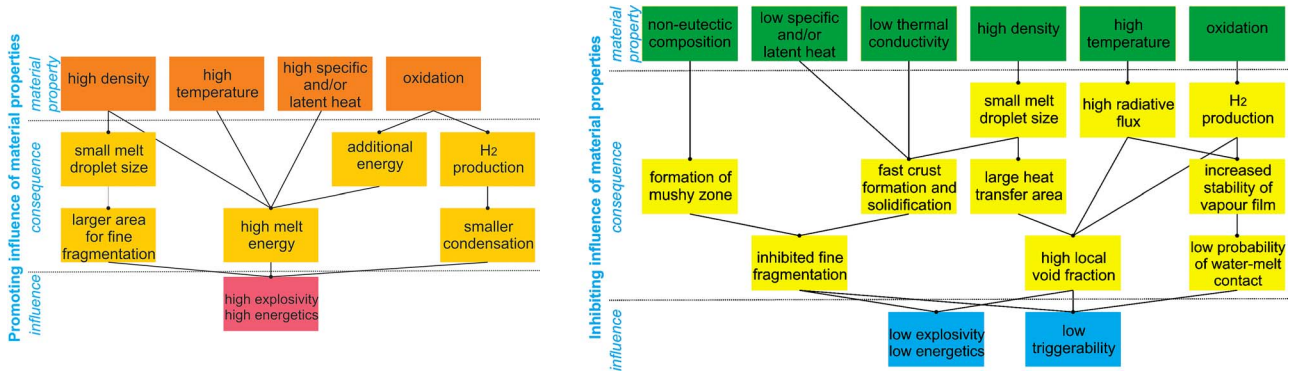

Fig. 1 Promoting (left) and inhibiting (right) influence of material properties on the steam explosion [5,7]

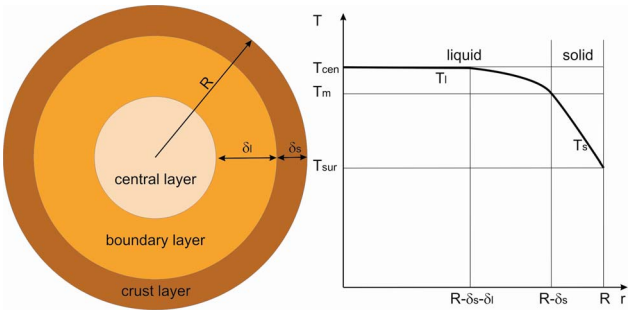

Fig. 2 HTMOD

is divided into the liquid part, where the temperature profile T_l is above the melting temperature T_m, and into the solid part, where the temperature profile T_s is below the melting temperature. In both parts the thermal conductivity and the density are considered to be equal and constant.

The temperature profile inside the central layer is considered to be constant and equal to the initial temperature $T_{\text{cen}}[t=0]$ of the melt droplet when it was born (e.g., at jet breakup). By this assumption the time needed for the surface condition to progress inside the melt droplet was considered. The temperature profile inside the boundary layer with thickness δ_l is based on the parabolic representation. In the boundary layer the temperature is below the initial temperature but still above the melting temperature. The parabolic profile approximation can be obtained from the mathematical-physical model for a totally liquid or a totally solid opaque droplet by assuming quasistatic conditions, where the temperature change does not depend on the radial coordinate r. The temperature profile in the crust layer on the melt droplet surface with thickness δ_s is considered to be linear if a liquid core is still present. The linear profile approximation can be obtained from the mathematical-physical model for opaque droplets by assuming that the thickness of the crust layer is constant (latent heat is assumed to be infinitive) and significantly lower than the radius of the melt droplet, and that the liquid core is at the melting temperature (acting like a heat source). Once the melt droplet is completely solid the parabolic profile presentation is assumed. These profile assumptions are reasonable and result in a good agreement of the established temperature profile with the exact solution of the mathematical-physical model, as presented in Ref. [10]. The temperature profiles used in HTMOD can be written as

$$T_l[r,t] = \begin{cases} T_{\text{cen}}[t], & r \le R - \delta_s[t] - \delta_l[t] \\ T_{\text{cen}}[t] - \dfrac{T_{\text{cen}}[t] - T_{\text{int}}[t]}{\delta_l[t]^2} \cdot (r - R + \delta_s[t] + \delta_l[t])^2, & R - \delta_s[t] - \delta_l[t] < r \wedge r \le R - \delta_s[t] \end{cases}$$

$$T_s[r,t] = \begin{cases} T_m + \dfrac{T_{\text{sur}}[t] - T_m}{\delta_s[t]}(r - R + \delta_s[t]), & R - \delta_s[t] < r \wedge r \le R \\ T_{\text{cen}}[t] - \dfrac{T_{\text{cen}}[t] - T_{\text{sur}}[t]}{R^2} r^2, & r \le R \wedge \delta_s[t] = R \end{cases}$$

$$T_{\text{cen}}[t] = \begin{cases} T_{\text{cen}}[t=0], & \delta_l[t] \ne R - \delta_s[t] \\ T_{\text{cen}}[t], & \delta_l[t] = R - \delta_s[t] \end{cases}, \quad T_{\text{int}}[t] = \begin{cases} T_{\text{sur}}[t], & \delta_s[t] = 0 \\ T_m, & \delta_s[t] \ne 0 \end{cases} \tag{2}$$

where T_{int} is the temperature between the boundary and the crust layer (if the crust layer is present) or the droplets' surface temperature T_{sur} (if the crust layer is absent). As seen in Eq. (2), the temperature profiles are in general a function of four model parameters, which have to be calculated to characterize the conditions inside the melt droplet. These parameters are T_{cen} (in case that the central layer is absent) or δ_l (if the central layer is present), δ_s, T_{sur}, and R. The HTMOD model parameters must be determined in a way that satisfies the heat balance equation

$$\frac{dQ}{dt} = -4\pi R^2 q[t] \tag{3}$$

where Q is the internal energy of the melt droplet, and the boundary condition for the temperature profile gradient

$$q[t] = \begin{cases} q_l[R,t], & \delta_s[t] = 0 \\ q_s[R,t], & \delta_s[t] \ne 0 \end{cases}$$

$$q_s[r,t] = -\lambda \frac{\partial T_s}{\partial r}, \quad q_l[r,t] = -\lambda \frac{\partial T_l}{\partial r} \tag{4}$$

which has to result in a heat flux equal to the heat flux from the melt drop surface to the surrounding water.

3 Fragmentation Process

3.1 Discussion. Figures 3 and 4 show the HTMOD simulation results in comparison to the exact NS for opaque melt droplets (see Eq. (1)) and typical premixing conditions [10]. The heat flux from the melt droplet surface was determined as the sum of the film boiling heat flux and the radiation heat flux. The simulation results are shown for typical prototypic corium ($R=1$ mm) and simulant alumina ($R=10$ mm) melt droplets, created during the premixing phase in typical steam explosion experiments [4]. Homogeneous initial temperatures are chosen based on typical experimental conditions and are set to 2700 K for alumina, 3000 K for corium, and 300 K for water [4]. The material properties used in the simulations are listed in Table 1.

Figure 3 demonstrates the temperature profile development in time. It can be seen from the NSs that the temperature profiles in the solid layer on the droplet surface are almost linear during the initial crust growth. As seen in Figs. 3 and 4, the linear profile

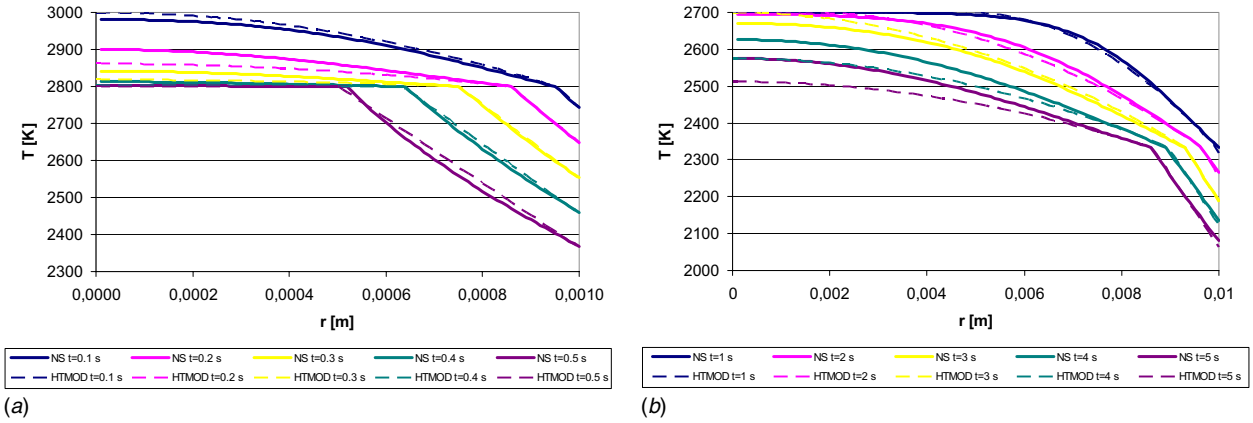

(*a*) (*b*)

Fig. 3 Temperature profiles for corium (*a*) and alumina (*b*) at different times

approximation in HTMOD gives rather good results in this initial stage. The discrepancies in the crust growth increase in the final period of the solidification. But this is not an important model limitation of HTMOD, since we are interested mainly in the initial growth of the solid crust, which influences the ability of the melt droplet fragmentation already before the droplet is significantly solidified.

Within some hundredths or tenths of a second, the velocities of the typical experimentally created corium or alumina melt droplets, respectively, are near the critical velocities necessary for the fragmentation of the liquid melt droplets during the premixing phase. Since at the same time scale also the crust, which increases the surface stiffness, is being created for corium melt droplets, it may be assumed that once the crust starts to grow, the corium melt droplet cannot fragment anymore during typical premixing experiments. Consequently for the conditions of typical experiments with corium melts we do not need to develop fragmentation criteria for partially solidified melt droplets (i.e., whether a partially solidified melt droplet will fragment or not due to the act of hydrodynamic forces) during premixing. For alumina droplets the crust formation is significantly delayed in comparison to corium droplets. Since the delay is longer than the time of the melt droplet deceleration, it may be again considered that once the crust is being created, the alumina melt droplet cannot fragment anymore. But in reactor applications the premixing conditions may be different; therefore fragmentation criteria for partially solidified melt droplets are needed also for the premixing phase.

If the typical premixing time of the order of 1 s is taken into account [4], we realize based on Fig. 4 that at that time the early born corium melt droplets are already totally frozen and as such cannot be actively involved in the steam explosion process. On the other hand alumina melt droplets and lately born corium droplets, which are still liquid or only partly solidified, can be actively involved in the steam explosion process. Therefore the development of fragmentation criteria is important for the explosion phase in typical experiments and in reactor applications.

3.2 Experimental Results. The effect of the melt droplets' surface solidification on the fragmentation was experimentally investigated in Refs. [11–13], where eutectic Wood metal alloy and eutectic Pb–Bi alloy were employed. In Ref. [11] the crust thickness was around 100 μm during the experiments, whereas in Refs. [12,13] the crust thickness was a few μm. However, only a detailed report of Ref. [11] enables us to make quantitative and qualitative analyses of experimental data.

In the performed experiments in Ref. [11] the melt droplets of Wood metal were dropt into the test channel filled with water, and the hydrodynamic fragmentation was induced by a strong water flow. By choosing the melt droplets' temperature in the range 75–159°C, the water's temperature in the range 10–75°C, and the melt droplets' radius in the range 1.6– 2.9 mm, the crust thickness at the onset of the water flow was varied. Water flows of up to approximately 40 m/s were produced inside the test channel. In total 65 experiments were performed.

In Fig. 5 the experimental results on the fragmentation behavior are given for various water velocities and crust thicknesses. Although the relative velocities are commonly used for correlating the fragmentation behavior, the water velocities are used herein since only those values were explicitly given for all experiments. The difference between the water and relative velocities at the time of the fragmentation onset was up to approximately 6 m/s for the highest water velocities [11]. The crust thickness of the melt

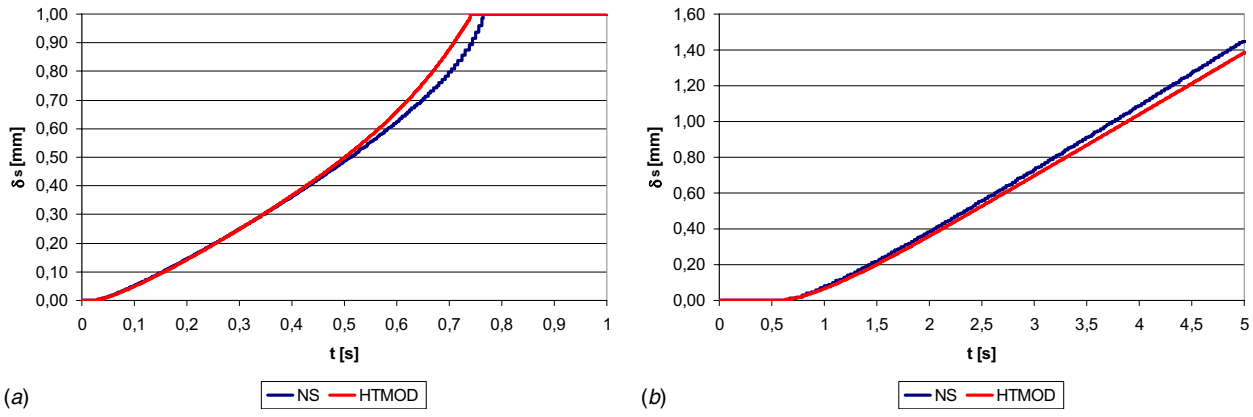

(*a*) (*b*)

Fig. 4 Crust layer thickness time evolution for corium (*a*) and alumina (*b*)

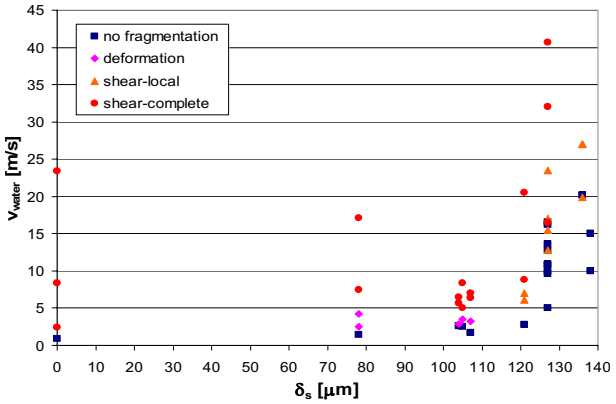

Fig. 5 Map of melt droplet fragmentation phenomena for various water velocities depending on crust thickness [11]

droplet was calculated using a heat transfer model, assuming a symmetric sphere and determining the heat transfer to the surrounding water by a correlation for forced convection heat transfer. The results in Fig. 5 show an existence of two regions, a region where the crust thickness is small enough to be flexible and a region where the crust thickness is thick enough to show more solid behavior. The transition between the regions occurs in a very narrow range of the crust thickness, at around 105–125 μm, and is due to the drastic transition in the fragmentation behavior, which could be described by a sudden occurrence of drop stability against deformation above the limiting crust thickness. The effect of an increased crust thickness does not appear to be sufficient for the explanation of the increased stability; therefore effects of material properties during the crust growth have to be considered [11]. For a crust thickness below the critical value and at smaller water velocities the melt droplet fragmented by deformation. At higher velocities local fragmentation of the melt droplet was due to shear flow effects. With increasing velocities a complete fine fragmentation appeared and was also due to the shear flow effect. When the crust thickness was above the critical value the fragmentation occurred only by shear flow effects, which underline that flexible crusts existed in the region with fragmentation by deformation. With increasing water velocities the complete fine fragmentation due to the shear flow seems to dominate more and more.

3.3 Fragmentation Criteria. For the liquid melt droplets the Weber number is commonly used to characterize different regions of the hydrodynamic fragmentation

$$\mathrm{We} = \frac{\rho_c v_{\mathrm{rel}}^2 D}{\sigma} \tag{5}$$

where ρ_c is the coolant density, v_{rel} is the relative velocity between the melt droplet and the coolant, D is the diameter of the melt droplet, and σ is the surface tension. The Weber number relates the hydrodynamic force acting to destroy the melt droplet, and the surface tension force acting to retain the melt droplet form. If the Weber number exceeds the critical value, the melt droplet fragments into smaller and more stable melt droplets. The most commonly used critical value is 12. Once a crust is created on the melt droplet surface, the role of surface tension is replaced with the stabilizing forces of the solid crust. Therefore the use of the Weber number can no longer be a good fragmentation criterion for partly or totally solidified melt droplets.

The experimental results in Fig. 5 serve to give some insight into possible limiting fragmentation mechanisms for melt droplets with a crust as well as the theoretical approaches to describe them. As given schematically in Fig. 6 two fragmentation mechanisms are discussed herein. Since we are interested in droplet conditions, when the crust thickness is significantly lower compared with the

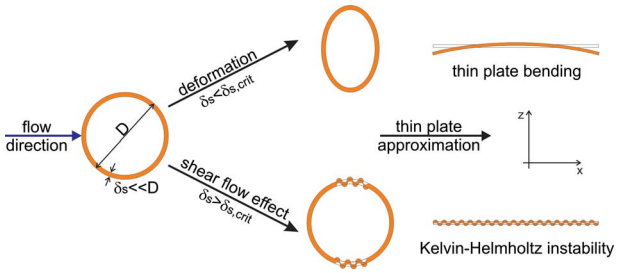

Fig. 6 Schematic view of droplets' solid layer fragmentation mechanisms

melt droplets' diameter, the thin plate approximation is used in the theoretical discussion. The energy E_{tp} of the deformed thin plate is

$$E_{\mathrm{tp}} = \frac{E\delta_s^3}{24(1-\mu^2)} \int \int_S \left(\frac{\partial^2 \zeta}{\partial x^2}\right)^2 dS = C \cdot I \tag{6}$$

where I is the integral of the second derivate of the deformation ξ along the x axis of the thin plate, S is the surface area of the thin plate, and C is the crust stiffness, which depends on the crust thickness δ_s, Young's modulus E, and Poisson's ratio μ. When the deformation is due to bending, the value of the integral I in Eq. (6) can be related to the maximal strength of the thin plate [11]

$$I_{\mathrm{def}} = \frac{16\Sigma_{\max}^2(1-\mu^2)^2}{E^2\delta_s^2} S \tag{7}$$

where S is the surface area of the considered melt droplet and $\Sigma_{\max}$ is the maximal tensile strength.

Considering the maximal thin plate bending due to outside water flow, a modified Weber number for fragmentation of the melt droplet by deformation due to bending may be defined based on Eqs. (6) and (7),

$$\mathrm{We}_{\mathrm{def}}^* = \frac{\rho_c v_{\mathrm{rel}}^2 DE}{\Sigma_{\max}^2 \delta_s (1-\mu^2)} \tag{8}$$

On the other hand the shear flow effects are treated according to the Kelvin–Helmholtz instability growth on the thin plate surface. The corresponding modified Weber number may be defined as

$$\mathrm{We}_{\mathrm{KH}}^* = \frac{\rho_c v_{\mathrm{rel}}^2 D^3}{E\delta_s^3}(1-\mu^2) \tag{9}$$

where the prevailing effect of the relative velocity over the crust stiffness is considered. The background of Eq. (9) could be also seen from Eq. (6).

The agreement of the suggested mechanisms with experimental results from Fig. 5 can be seen in Fig. 7. Equation (8) or Eq. (9) was used for the fragmentation criteria definition in case the crust thickness was lower or higher than the critical value, respectively. The critical modified Weber number is obtained by considering Wood's metal properties being constant during the crust growth (e.g., independent of temperature) and equalizing the relative velocities to the water velocity (see discussion in Sec. 3.2)

$$\mathrm{We}_{\mathrm{crit}}^* \approx \begin{cases} 9, & \delta_s \le \delta_{s,\mathrm{crit}} \\ 0.1, & \delta_s > \delta_{s,\mathrm{crit}} \end{cases} \tag{10}$$

where $\delta_{s,\mathrm{crit}}$ is the critical crust thickness, which is assumed to depend on material properties (see discussion in Sec. 3.2).

The agreement between the theory and the experiments is not conclusive. Because of the restricted number of experiments, the critical velocities and the modified Weber number for onsetting fragmentation or the velocities indicating the transition in the fragmentation behavior could be determined only roughly. Additionally, the observed drastic change in the fragmentation behavior between the two regions needs further investigations.

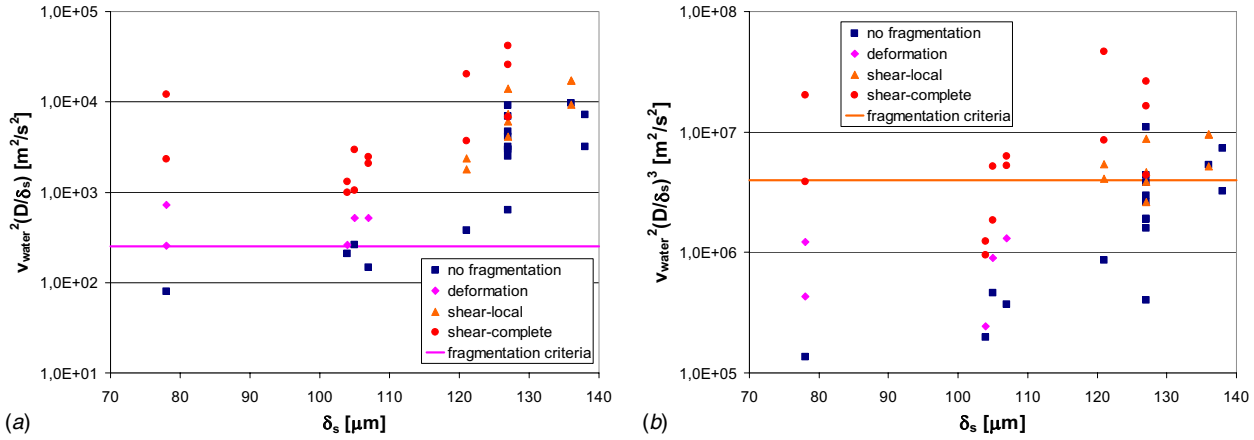

Fig. 7 Deformation (*a*) and shear (*b*) fragmentation criteria used for crust thicknesses smaller (*a*) and larger (*b*) than the critical crust thickness

3.4 Fragmentation Time Scale. The few available experiments in Ref. [11] weakly indicate that the fragmentation time is around 1 ms regardless of the crust thickness. Therefore experimental results indicate that a much smaller instability growth is necessary for the crust to break up due to shear flow effects if compared with the breakup of the more flexible liquid melt droplet.

The experimentally obtained fragmentation times were compared with the Pilch correlation for the total breakup period (i.e., fragmentation time) of droplets in a liquid-gas system [14]. Although the Pilch correlation gives up to three times longer fragmentation times compared with experimentally obtained ones, it enables a quantitative description of experimental results.

It is obvious that additional experiments would be needed to be able to correlate the influence of the crust thickness on the melt droplet breakup time.

4 Transport Equations

To enable the use of the developed HTMOD and the fragmentation criteria in FCI computer codes with an Eulerian description, adequate transport equations for the decisive model parameters were derived in conservative form.

HTMOD is characterized with four parameters (see Eq. (2)). Therefore, four melt droplet quantities of primary importance with corresponding equations must be introduced in order to make a mathematical closed system of equations. The considered melt droplet quantities of primary importance are as follows: melt droplets' internal energy, surface area, surface stiffness, and surface heat flux. The variation of the internal energy is covered by the energy conservation equation, which is already included in FCI codes [6]. The second important quantity is the melt droplet surface area, which defines the heat transfer and the source for the melt droplet fragmentation. Generally, the interfacial area transport equation is used in FCI codes [6]. The third important melt droplet quantity is the surface stiffness, which influences the ability of the melt droplet to fragmentize and therefore significantly affects the FCI process. The effect of the surface stiffness is described with Eq. (6), where the surface stiffness C is a function of material properties and the crust thickness. Therefore, the variation of the crust thickness is treated by the general conservative transport equation for Φ_δ as follows:

$$\frac{\partial \Phi_\delta}{\partial t} + \nabla(\Phi_\delta \vec{u}) = \Gamma_\delta$$

$$\Phi_\delta = \frac{\delta_s^3}{V_{\text{cell}}} = \frac{\delta_s^3}{V/\alpha_d} = 6\alpha_d \frac{\delta_s^3}{\pi D^3} \tag{11}$$

where $\vec{u}$ is the velocity field and Φ_δ is the transported quantity, representing here the crust stiffness in the mesh cell with the volume V_{cell}. Φ_δ can be also considered as the capability of the melt droplet to sustain melt droplet fragmentation. Material properties as Young's modulus and Poisson's ratio are assumed to be constant. α_d, A, and V are the droplets' volume fraction, the surface area, and the volume, respectively. Γ_δ is the source term, where the influence of the melt droplet quenching determined from HTMOD (see Sec. 2), melt droplet coarse fragmentation, jet breakup, and melt droplet coalescence should be considered. The last important melt droplet quantity is the melt droplet surface heat flux to the surrounding coolant. The surface heat flux is directly influencing important FCI processes, as the solid crust formation, the void fraction, and the stability of the vapor film surrounding the melt droplet surface. The heat flux is a function of the surface temperature gradient. To conserve the heat flux on the melt droplet surface an adequate conservative transport equation for Φ_T was derived as follows:

$$\frac{\partial \Phi_T}{\partial t} + \nabla(\Phi_T \vec{u}) = \Gamma_T$$

$$\Phi_T = \begin{cases} \dfrac{q_l A}{V_{\text{cell}}} = \dfrac{q_l A}{V/\alpha_d} = 6\alpha_d \dfrac{q_l}{D}, & \delta_s = 0 \\ \dfrac{q_s A}{V_{\text{cell}}} = \dfrac{q_s A}{V/\alpha_d} = 6\alpha_d \dfrac{q_s}{D}, & \delta_s \neq 0 \end{cases} \tag{12}$$

The influence of melt droplet quenching, melt droplet coarse fragmentation, jet breakup, and melt droplet coalescence is considered in the source term Γ_T.

5 Conclusions

In FCI modeling the melt solidification process, which can prevent further melt fragmentation, should be taken into account. The melt droplet heat transfer models used in FCI codes are generally basic and are as such not capable to appropriately predict the observed differences between simulant and prototypic materials. Therefore the heat transfer model for opaque melt droplets (denoted as HTMOD) was developed with the purpose to significantly improve the accuracy of the calculated steam explosion energetics. HTMOD is complex enough that the material properties can be adequately considered. With HTMOD the growth of the crust, which limits the melt droplets' fragmentation during the

premixing and explosion phases and thus significantly influences the steam explosion energetics, can be accurately predicted. At the same time HTMOD is simple enough that it can be practically implemented into FCI codes, thus being an optimal model for FCI applications. Additionally, fragmentation criteria taking into account the influence of the formed crust on the fragmentation process have been derived. The developed fragmentation criteria are based on experimental results and they are derived in a way to be independent of material properties. Due to the limited number of performed experiments the fragmentation criteria could be determined only roughly. Adequate transport equations for most important model quantities were derived in order to enable the use of the developed models and criteria in FCI computer codes with an Eulerian description.

Acknowledgment

The authors acknowledge the support of the Ministry of Higher Education, Science and Technology of the Republic of Slovenia within the cooperative CEA-JSI research project (Contract No. 1000-08-380001) and Research Program No. P2-0026. The Jožef Stefan Institute is a member of the Severe Accident Research Network of Excellence (SARNET2) within the 7th EU Framework Program.

References

[1] Sehgal, B. R., 2006, "Stabilization and Termination of Severe Accident in LWRs," Nucl. Eng. Des., **236**, pp. 1941–1952.
[2] Cizelj, L., Leskovar, M., and Končar, B., 2006, "Vulnerability of a Partially Flooded PWR Reactor Cavity to a Steam Explosion," Nucl. Eng. Des., **236**, pp. 1617–1627.
[3] Leskovar, M., 2009, "Pressure Load Estimation During Ex-Vessel Steam Explosion," ASME J. Eng. Gas Turbines Power, **131**(3), p. 032901.
[4] Huhtiniemi, I., Magallon, D., and Hohmann, H., 1999, "Results of Recent KROTOS FCI Tests: Alumina Versus Corium Melts," Nucl. Eng. Des., **189**, pp. 379–389.
[5] Leskovar, M., Meignen, R., Brayer, C., Bürger, M., and Buck, M., 2007, "Material Influence on Steam Explosion Efficiency: State of Understanding and Modelling Capabilities," The 2nd European Review Meeting on Severe Accident Research (ERMSAR-2007), Jun. 12–14, FZK, Karlsruhe, Germany.
[6] Meignen, R., and Picchi, S., 2005, "MC3D Version 3.5: User's Guide," IRSN, Report No. NT/DSR/SAGR/05-84.
[7] Dinh, T. N., 2007, "Material Property Effect in Steam Explosion Energetics: Revised," The 12th International Topical Meeting on Nuclear Reactor Thermal Hydraulics (NURETH-12), Pittsburgh, PA, Sept. 30–Oct. 4, pp. 1–19, Log No. 150.
[8] Dombrovsky, L. A., and Dinh, T.-N., 2008, "The Effect of Thermal Radiation on the Solidification Dynamics of Metal Oxide Melt Droplets," Nucl. Eng. Des., **238**, pp. 1421–1429.
[9] Meignen, R., Magallon, D., Bang, K. H., Berthoud, G., Basu, S., Bürger, M., Buck, M., Corradini, M. L., Jacobs, H., Melikhov, O., Naitoh, M., Moriyama, K., Sairanen, R., Song, J. H., Suh, N., and Theofanous, T. G., 2005, Comparative Review of FCI Computer Models Used in the OECD-SERENA Program," *Proceedings of the ICAPP 2005*, Seoul, South Korea, May, pp. 15–19.
[10] Uršič, M., and Leskovar, M., 2008, "Modelling of Material Properties Influence on Steam Explosion Energetics," *Proceedings of the International Conference Nuclear Energy for New Europe*, Portorož, Slovenia, Sept. 8–11.
[11] Bürger, M., Cho, S. H., Kim, D. S., Carachalios, C., Müller, K., and Fröhlich, G., 1985, "Effect of Solid Crust on the Hydrodynamic Fragmentation of Melt Droplets," Institut für Kernenergetik und Energiesysteme der Universitat Stuttgart, Report No. IKE 2 TF-74.
[12] Haraldsson, H. Ó., Li, H. X., Yang, Z. L., Dinh, T. N., and Sehgal, B. R., 2001, "Effect of Solidification on Drop Fragmentation in Liquid-Liquid Media," Heat Mass Transfer, **37**, pp. 417–426.
[13] Yang, J. W., and Bankoff, S. G., 1987, "Solidification Effects on the Fragmentation of Molten Metal Drops Behind a Pressure Shock Wave," ASME J. Heat Transfer, **106**, pp. 226–231.
[14] Kolev, N. I., 2002, *Multiphase Flow Dynamics 2; Mechanical and Thermal Interactions*, Springer-Verlag, Berlin.